IRBM 45 (2024) 100820

Contents lists available at ScienceDirect

IRBM

journal homepage: www.elsevier.com/locate/irbm

Elsevier Masson France

EM|consulte

www.em-consulte.com

Original Article

Improved Estimation of Elbow Flexion Angle from IMU Measurements Using Anatomical Constraints

Anna Bicchi *, Alessandro Colombo [1]

Department of Electronics, Information, and Bioengineering, Politecnico di Milano, Milano, Italy

HIGHLIGHTS

- Anatomical constraints leveraged for precise joint angle estimation.
- Error-state Kalman filter updates estimates, accounts for sensor orientation error.
- Experimental validation demonstrates superior accuracy compared to state-of-the-art methods.

GRAPHICAL ABSTRACT

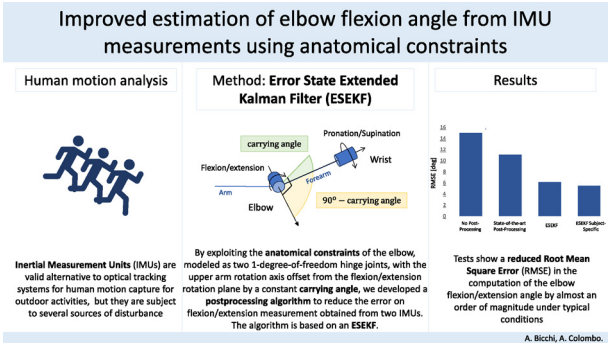

ARTICLE INFO

Article history:
Received 18 July 2023
Received in revised form 19 December 2023
Accepted 7 January 2024
Available online 17 January 2024

Keywords:
Human motion
Joint angle estimation
Inertial sensors
Anatomical constraints

ABSTRACT

Objectives: Inertial Measurement Units (IMUs) are a valid alternative to optical tracking systems for human motion capture, but they are subject to several disturbances that limit their accuracy. We aim to improve the accuracy of elbow joint angle estimation from IMU measurements by introducing a novel postprocessing algorithm that uses anatomical constraints and does not require any prior calibration or knowledge of anthropometric parameters.
Materials and Methods: We propose a new error model that addresses sensor misalignment and fusion errors. We use an error state extended Kalman filter (ESEKF) with state constraints to integrate the anatomical constraints. We validate the proposed algorithm by testing it in different scenarios and comparing it with a state-of-the-art optical tracking system.
Results: The research results highlight the superior performance of the proposed method compared with existing techniques. The study demonstrates a significant reduction in errors, particularly in complex arm movements and under strong external disturbances. The results obtained in the three different tested scenarios underscore the robustness and effectiveness of the developed algorithm, reaching half the error committed by the existing calibration-free correction algorithms proposed in the literature.
Conclusions: The developed technique provides highly accurate estimates of joint angles in several challenging real-world scenarios.

1. Introduction

Tracking the motion of human limbs has a fundamental role in human performance assessment, health, and rehabilitation monitoring applications [1–3]. Optical tracking systems have long been considered the gold standard for human motion analysis. However,

* Corresponding author.
E-mail addresses: anna.bicchi@polimi.it (A. Bicchi), alessandro.colombo@polimi.it (A. Colombo).
[1] Anna Bicchi and Alessandro Colombo are with the Dipartimento di Elettronica Informazione e Bioingegneria, Politecnico di Milano, via Ponzio 34/5. 20133, Milano, Italy.
https://doi.org/10.1016/j.irbm.2024.100820

they need a carefully calibrated laboratory environment, making their application impractical outdoors, and are very sensitive to lighting and visual occlusion [4].

Wearable sensors, specifically Inertial Measurement Units (IMUs), provide an exciting alternative since they enable data collection in real-life conditions [5,6]. IMUs utilize a gyroscope to detect their orientation in space. In the ideal case of an errorless gyroscope, this information alone would suffice to determine the changes in orientation of the IMU body. In practice, however, all gyroscopes are affected by more or less severe temporal drift, which must be compensated using information obtained from other sensors.

The IMUs that are typically used for motion analysis fuse, for this purpose, information from a MEMS gyroscope with the information provided by multiaxial accelerometers and magnetometers, enclosed in a small and lightweight package. Several sensor fusion algorithms have been presented in the literature, see e.g., [7–15]. When properly tuned, they all tend to yield comparable results [16]. Even though the fusion strategies differ, these sensor fusion algorithms typically exploit the low-frequency (gravitational) acceleration signal to correct roll and pitch angles, and the earth's magnetic field data to correct the yaw angle. Persistent external accelerations and local magnetic disturbances, together with gyroscopic drift, are therefore the main sources of error [17]. The effect of magnetic disturbances in particular tends to dominate when IMUs are used to measure human activities that don't involve significant persistent acceleration of the subject.

To improve the accuracy of the orientation estimate in human motion-tracking, when multiple IMUs are used to track the orientation of different body segments, it is possible to exploit kinematic models of the human body [18–20] to compensate for the error in one sensor's orientation with the information provided by another sensor. In [5,21–23], the Authors have exploited the kinematic constraints of the joints (knee or elbow) to improve the joint angle estimation. Except for [5,22], the above studies focus on the analysis of the knee joint, which is a hinge joint with one degree of freedom. Furthermore, they describe full acquisition protocols and data fusion algorithms utilizing the measures coming from one or more IMUs.

In this paper, we target the flexion angle of the elbow joint, which is a two-degree-of-freedom loose-hinge joint [24], using a two-IMUs setup taken from [22]. Inspired by previous work [25], which improved elbow flexion angle estimation using joint anatomical constraints, we employ a comparable mathematical expression of the elbow kinematic constraints. We develop an error model of the orientation errors due to IMU misalignment with body segments and external disturbances. Subsequently, a recursive filter is designed to estimate these errors, in the form of an Error State Extended Kalman Filter (ESEKF) with state constraints. One key innovation lies in our algorithm's ability to enhance joint angle accuracy without the need to perform any sort of calibration motion before data collection. Moreover, unlike most existing methods, ours does not rely on the subject's anthropometric measurements or precise alignment of the IMUs on the arm and can incorporate the subject's carrying angle.[2] This unique set of features allows seamless integration into existing data processing pipelines (or application to previously acquired data) without altering the acquisition protocol, something that is not possible even with the best-performing and most flexible algorithms in the literature, such as [22]. This paper provides a detailed explanation of our algorithm and evaluates its performance. To ensure a comprehensive assessment, we conducted tests in vivo, measuring elbow flexion angle on a human subject, and measuring the angle between IMUs fixed on a rigid support at various calibrated angles. Our algorithm's performance, both with and without information about the subject's carrying angle, is compared against raw data and the postprocessing algorithm proposed in [25]. Importantly, our approach is also validated against measurements acquired on a state-of-the-art passive-markers optical tracking system, with markers placed according to the Lobo-Prat protocol complying with the International Society of Biomechanics guidelines.

[2] see Sec. 2.1 for a definition.

2. Material and methods

2.1. Joint angle model

The human elbow joint is a compound of the humeroulnar and humeroradial joints and of the proximal and distal radioulnar joints. Their aggregate function can be approximated as the composition of two one-degree-of-freedom hinge joints, the first allowing flexion/extension, the second pronation/supination [26]. Note that, as described for instance in [5], the longitudinal axis of the distal segment (the forearm), which coincides with the pronation/supination rotation axis, is offset from the flexion/extension rotation plane. This offset angle is known as the *carrying angle*. At full extension, the carrying angle is known to vary between roughly 5 and 25 degrees [26,27], with differences between male and female, and between dominant and non-dominant arms. It changes also with the flexion angle, though the amount by which it changes is not well documented and depends on the considered definition of the carrying angle, which is itself not fully standardized [27]. In this work, we approximate the flexion/extension degree of freedom as a single hinge joint, and we assume that the carrying angle, defined as the angle between the longitudinal axis of the distal segment and the flexion/extension rotation plane, is constant. Referring to the proximal segment longitudinal axis as x_1 and to the distal segment longitudinal axis as x_2, we can define the elbow flexion angle, α, as

$$\alpha \triangleq \arccos\left(\frac{x_1^\top x_2}{\|x_1\|\|x_2\|}\right). \tag{1}$$

Furthermore, we assume that the proximal segment lays in the flexion/extension rotation plane so that the flexion angle (the angle between proximal and distal segments) coincides with the carrying angle at full extension. This is consistent with the more common definition of the carrying angle [27], and provides a relatively simple way to measure it on a human subject by means of a goniometer.

2.2. Error model

Our algorithm assumes that the two IMUs are positioned as proposed in [22], by aligning their x axis with the corresponding body segment longitudinal axis. Referring to Fig. 1, $Sensor_1$ is positioned on the upper arm and $Sensor_2$ on the wrist. $Sensor_1$ is positioned over the central third of the humerus, slightly posterior to avoid additional errors due to the shoulder rotations and skin motion artifacts. $Sensor_2$ is positioned over the distal, flat surface of the radius and ulna, with the local x axis pointing towards the hand, to minimize soft tissue artifacts. Note that, with this positioning, the two sensors' relative position is subject to both of the elbow's degrees of freedom. With reference to Fig. 1, assuming that $Sensor_1$ is worn so that its z-axis is (approximately) parallel to the flexion/extension rotation axis, the angle between the x-axis of $Sensor_2$, i.e., x_2, and the z-axis of the upper $Sensor_1$,

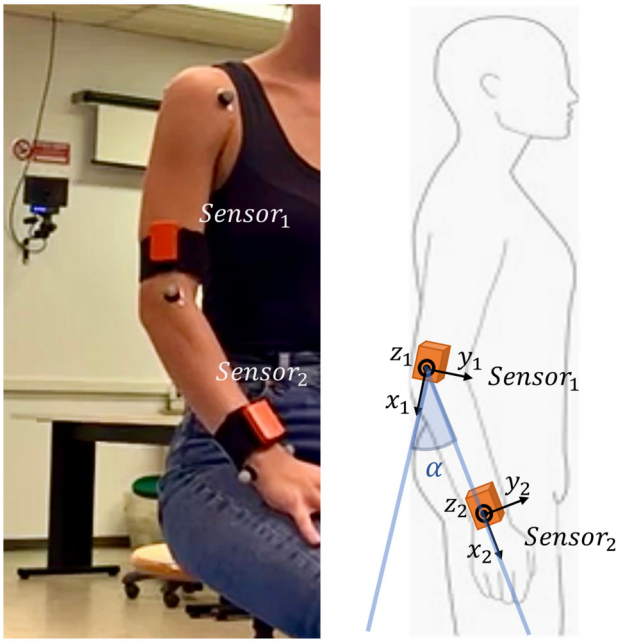

Fig. 1. Sensors and markers configurations on the subject.

i.e., z_1, is equal to β, where $90-\beta$ degrees is the carrying angle. The assumption we made of constant carrying angle, can be then mathematically expressed by assuming that z_1 and x_2 are unit vectors, and imposing that the scalar product of the two vectors (henceforth referred to as ϵ) is equal to

$$\epsilon \triangleq z_1^\top x_2 = \cos(\beta). \tag{2}$$

The orientations of $Sensor_1$ and $Sensor_2$ are estimated at each time step by the IMU sensors fusion algorithms and are expressed as rotation matrices with respect to the global frame. In particular, from now on, R_{1g} expresses the orientation of $Sensor_1$, and R_{2g} the orientation of $Sensor_2$. Accordingly, equation (2) can be rewritten as:

$$\epsilon = (R_{1g}z)^\top R_{2g}x = \cos(\beta), \tag{3}$$

where $x \triangleq [1\ 0\ 0]^\top$, $z \triangleq [0\ 0\ 1]^\top$. In the considered scenario, two factors may contribute to the erroneous measurement of z_1 and x_2:

(E1) the misalignment of the IMU with the anatomical axis, or
(E2) sensor fusion errors in the matrices R_{ig}.

We can correct the two sources of error using two kinds of correction matrices:

- For correction (E1), local correction matrices R_{1lc} and R_{2lc} are used to rotate vectors z and x within their respective reference frames.
- To address (E2) a global correction matrix R_c is employed to rotate the relative orientation of the reference frames of the two IMUs.

It is then possible to express the constraint (3) including all corrections as

$$\epsilon = (R_c R_{1g} R_{1lc} z)^\top R_{2g} R_{2lc} x = \cos(\beta). \tag{4}$$

The correction matrices R_c, R_{2lc} are expressed in the Roll Pitch Yaw (RPY) representation, while R_{1lc} is expressed in Yaw Pitch Roll (YPR):

Table 1
Elements of the state vector ξ of the ESEKF.

Correction angle	Rotation axis
θ_1	y_1 axis in $Sensor_1$ frame
ψ_1	x_1 axis in $Sensor_1$ frame
θ_2	y_2 axis in $Sensor_2$ frame
ϕ_2	z_2 axis in $Sensor_2$ frame
θ	y axis in global frame
ϕ	z axis (vertical) in global frame
ψ	x axis in global frame

$$R_{1lc} = \begin{bmatrix} \cos\theta_1 & \sin\theta_1\sin\psi_1 & \sin\theta_1\cos\psi_1 \\ 0 & \cos\psi_1 & -\sin\psi_1 \\ -\sin\theta_1 & \cos\theta_1\sin\psi_1 & \cos\theta_1\cos\psi_1 \end{bmatrix},$$

$$R_{2lc} = \begin{bmatrix} \cos\theta_2\cos\phi_2 & -\sin\phi_2 & \cos\phi_2\sin\theta_2 \\ \sin\phi_2\cos\theta_2 & \cos\phi_2 & \sin\phi_2\sin\theta_2 \\ -\sin\theta_2 & 0 & \cos\theta_2 \end{bmatrix},$$

$$R_c = \begin{bmatrix} \cos\theta\cos\phi & \cos\phi\sin\theta\sin\psi - \sin\phi\cos\psi & \cos\phi\sin\theta\cos\psi + \sin\phi\sin\psi \\ \sin\phi\cos\theta & \sin\phi\sin\theta\sin\psi + \cos\phi\cos\psi & \sin\phi\sin\theta\cos\psi - \cos\phi\sin\psi \\ -\sin\theta & \cos\theta\sin\psi & \cos\theta\cos\psi \end{bmatrix} \tag{5}$$

where ψ, θ, and ϕ are rotations around the IMU x, y, and z axis, respectively. Assuming that correction angles are small, the chosen representations are well suited, since they have singularities when $\theta = \pi/2$ and when $\theta = 3\pi/2$, away from where our correction matrices are expected to operate. In particular, in (5), R_{1lc} is the result of the combination of rotations around z_1, y_1, and x_1 axis of $Sensor_1$ in this order, and R_{2lc} is the result of the combination of rotations around x_2, y_2, and z_2 axis of $Sensor_2$ in this order. The order in which the rotations in R_{1lc} and R_{2lc} are applied has been chosen to perform the first rotation of each reference frame around the axis it is applied to, i.e., z for $Sensor_1$ and x for $Sensor_2$ (see (3)). This representation allows us to get rid of the correction angle ϕ_1 in R_{1lc}, and ψ_2 in R_{2lc}, obtaining a simpler model without loss of generality. By rotating the vectors z and x within their frames, the local correction matrices R_{1lc} and R_{2lc} have the effect of correcting the relative orientations of the IMUs with respect to the anatomical axes. The global correction matrix R_c, on the other hand, modifies the orientation of IMU 1 in the global frame. In the global frame, errors due to misalignment of an IMU with the anatomical axes are seen as rapidly changing signals, while sensor fusion errors, which directly affect the IMU's representation of the global frame, are slowly changing signals. The global correction matrix R_c is therefore more sensitive to the latter, and its contribution is chiefly in correcting sensor fusion errors.

2.3. Error state extended Kalman filter design

As anticipated, we use an ESEKF to estimate the error angles that characterize the three correction matrices. A standard Extended Kalman Filter for sensor fusion is designed to estimate a nonlinear process' state (e.g., the orientation and angular rates of the IMU) from the readings of the sensors (e.g., angular accelerations from a MEMS gyroscope, orientations from accelerometer and magnetometer). An ESEKF instead is designed to estimate the error between such a process' state and its true value. By estimating the error rather than the state, the ESEKF operates on a signal with lower-frequency dynamics. Additionally, acting on a small signal, its performance is less penalized by the process nonlinearity.

We designed an ESEKF with state constraints collecting the error angles in vector $\xi \triangleq \begin{bmatrix}\theta_1 & \psi_1 & \theta_2 & \phi_2 & \theta & \phi & \psi\end{bmatrix}^\top$, whose meanings are reported in Table 1. The error dynamics model subject to the constraint coming from (4) therefore becomes

$$\xi_k = \xi_{k-1} + v_{k-1} \tag{6a}$$

$$y_k = g(\xi_k) + \eta_k \triangleq (R_c \hat{R}_{1g} R_{1lc} z)^\top (\hat{R}_{2g} R_{2lc} x) - \cos(\beta) + \eta_k \tag{6b}$$

$$\text{s.t. } y_k = 0 + \eta_k, \tag{6c}$$

where subscript k is the time step, while v denotes the noise acting on the state evolution (6a). Equations (6b) and (6c) together express constraint (4), with the small Gaussian noise η modeling deviations from our kinematic model. In (6b), we omitted the dependence of the rotation matrices on k for the sake of conciseness. The ESEKF with state constraints is then designed as follows:

Prediction step:

$$\begin{aligned} \xi_k^- &= \xi_{k-1}, \\ P_k^- &= P_{k-1} + Q, \end{aligned} \tag{7}$$

Correction step:

$$\begin{aligned} K_k &= P_k^- C_k^T (C_k P_k^- C_k^T + R)^{-1}, \\ \xi_k &= \xi_k^- + K_k(\zeta - g(\xi_k^-)),\ \zeta \triangleq 0, \\ P_k &= (I - K_k C_k) P_k^-. \end{aligned} \tag{8}$$

Here, P is the state error covariance matrix; Q is the process noise covariance matrix; R is the variance of η; C is obtained at every time step as $\frac{\partial g(\xi)}{\partial \xi}\Big|_{\xi=\xi_k^-}$, where $g(\xi)$ is defined in (6b), and K is the Kalman gain. Constant ζ represents the observation made at each step k of the process output y_k. Imposing the observation equality $\zeta = 0$ allows us to integrate the constraint (6c) in the filter dynamics.

Using the elements of ξ_k as angles in the correction matrices (5) we can finally correct the two IMUs' rotation matrices as

$$\begin{aligned} R_{1corrected} &= R_c \hat{R}_{1g} R_{1lc}, \\ R_{2corrected} &= \hat{R}_{2g} R_{2lc}, \end{aligned} \tag{9}$$

where we omitted the dependence of the matrices on k for clarity.

2.4. Experimental setup

To validate the IMU-based joint angle measurements, we followed the typical procedure of comparing the results with those obtained from a passive-marker optical tracking system. This procedure is detailed in the following *Test 3*. Although optical tracking systems can precisely locate markers with sub-millimeter accuracy, joint angle estimates are inevitably affected by significant noise. The main sources of this noise are soft tissue artifacts [28] and errors resulting from imperfect alignment of markers with body segment axes. Therefore, to ensure a more reliable evaluation of the performance of our algorithm, we complemented this standard assessment with two further tests under conditions that eliminate the sources of inaccuracy present in optical tracking systems. Overall, we tested our algorithm in three different experimental setups detailed below.

Test 1: we evaluated the algorithm on a set of IMUs mounted on a wooden board at carefully calibrated angles. Six Xsens MTw IMUs (Xsens Technologies BV, Enschede, NL) were fixed on a wooden board as in Fig. 2. The orientation of each IMU was independently processed using XSens MT Manager 2021.4. $Sensor_1$ was used to represent the sensor on the subject's upper arm, while the others represented the sensor on the forearm in 5 different positions. The angle between the x axis of $Sensor_1$ and the x axis of each of the other sensors was measured with an electronic goniometer to be of 0°, 30°, 45°, 60°, 90°, with a resolution of 0.1°. The board was then moved in space by hand in an irregular waving

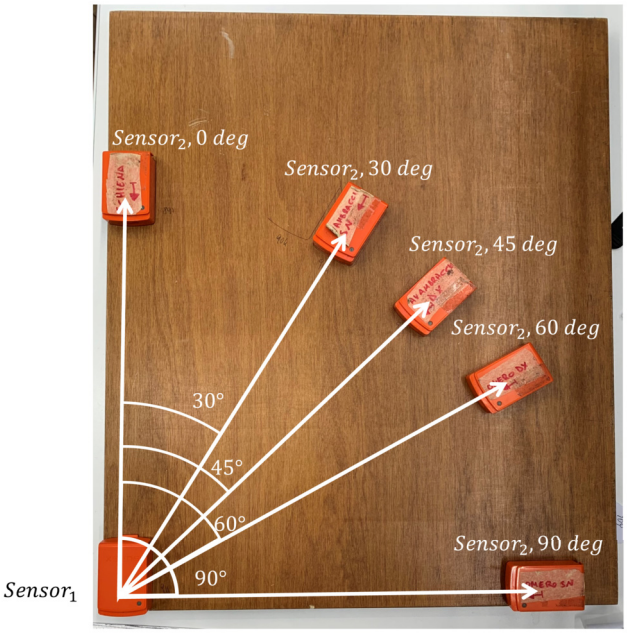

Fig. 2. First Test: Experimental set-up.

motion, ensuring that all axes explored the three degrees of freedom repeatedly. The orientation of each sensor was estimated by the Xsens Kalman Filter (XKF3) with a sampling rate of 100 Hz.

The proposed method was evaluated by comparing the results obtained by computing the joint angle, as expressed in (1),

1. using vectors x_1 and x_2 obtained from XKF3 without postprocessing,
2. using the vectors obtained through the postprocessing algorithm in [25],
3. using our postprocessing algorithm.

In the following, we refer to the three above methods of computation of the joint angle as NP (as No Postprocessing), LP (as Luinge Postprocessing), and EP (as ESEKF Postprocessing), respectively. When applying EP, we set $\beta = 90$ degrees, which corresponds to a carrying angle of 0 degrees. It is important to underline that having constant angles between IMUs during the tests did not give any unfair advantage to EP. Our algorithm, indeed, does not assume constant angles between sensors, and like the other two methods must obtain the angle measurement through the application of (1) to the time-varying estimates of x_1 and x_2. This test was carried out at the Leonardo Robotics Labs of Politecnico di Milano (www.deib.polimi.it/eng/lableo). The numerous robots, power lines, and metal structures in the lab generate significant magnetic interference and therefore provide a rather challenging environment for the IMUs.

Test 2: two of the same IMUs used in the previous experiment were worn by a subject on the right arm, positioned as in Fig. 1. The subject's right arm carrying angle at full extension was estimated, using an electronic goniometer aligned with the axes of the proximal and distal segments, to be equal to 16.4 degrees. The subject was asked to fully extend the elbow, and move the arm horizontally and vertically while maintaining the elbow fully extended. As in the first test, the orientation of each IMU was first computed using XKF3 and LP. We then tested our postprocessing algorithm with a carrying angle equal to 16.4 degrees ($\beta = 73.6$ degrees), as well as 0 ($\beta = 90$ degrees) to simulate the case where the subject anthropometry is not available at the time of data processing. We refer to the second postprocessing case as EP and to the first as EPSS, where SS stands for subject-specific. The test was

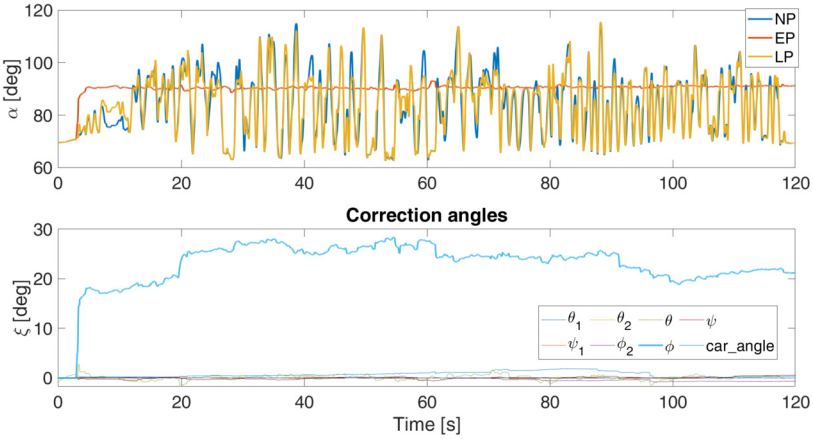

Fig. 3. Trajectory of α and ξ for $Sensor_1$ and $Sensor_2$ in *Test 1*, when the latter is placed at a 90 degrees angle.

repeated 4 times, and the measurement error was defined as the difference between the measured angle and the ground truth of 16.4 degrees since at full extension the elbow angle corresponds to the carrying angle. This test was carried out once again at the Leonardo Robotics Labs of Politecnico di Milano. The purpose of the test was to evaluate the effects of skin and soft-tissue artifacts, and the impact of the IMUs placement on a human arm, on the performance of the three methods, without the additional disturbances related to the optical tracking system.

Test 3: As the final test we performed a standard comparison of the four postprocessing methods, NP, LP, EP, and EPSS, against the measurement obtained from an optical tracking system. The same subject of Test 2 wore two IMUs on the right arm, positioned as in the second test, and was equipped with 6 retroreflective markers, positioned on the right arm on the posterior right shoulder, anterior right shoulder, lateral prominence of the elbow, medial prominence of the elbow, radial styloid (lateral prominence of the wrist), and ulnar styloid (medial prominence of the wrist), according to the protocol described in [29] (see Fig. 1), complying with the guidelines of the International Society of Biomechanics. Note that the protocol utilizes 26 markers located on both arms and on the torso. Since for this study we only needed to measure flexion/extension of the right elbow we used a subset of the full marker set. The protocol utilizes pairs of markers positioned on the measured joints to define a segment through the joint instantaneous center of rotation. The midpoint of the segment then approximates the center of rotation. The motion of the markers was acquired using a SMART DX 400 (BTS spa, Italy) optical tracking system with 8 cameras acquiring at 100 Hz. Marker trajectories were processed in Smart Analyzer (BTS spa, Italy). The subject executed 12 flexion/extension movements with her right arm while sitting on a stool. The laboratory where the optical tracking system is located has very few sources of magnetic disturbance and was, therefore, less challenging for the IMUs magnetometers.

In all the tests, we set matrix Q of EP and EPSS (see (7)) to a diagonal matrix with diagonal elements equal to [0.1015, 0.0202, 0.0369, 0.0530, 0.1278, 3.6109, 0.0308], while $R = 1$. In LP, the diagonal matrix Q had diagonal elements [1.42, 5.87, 5.58, 1.10, 6.20, 5.99] and $R = 0.175$. The elements of the Q matrices were optimized, for each of the postprocessing algorithms, to minimize the maximum RMS error over all performed tests. The value of R in LP was chosen according to [7].

3. Results

The experiment in *Test 1* consisted of a single trial lasting about 120 seconds and the full-time series was used in the analysis. The trajectory of the ESEKF state ξ, in the lower panel of Fig. 3, shows that the filter is correcting angle ϕ, which corresponds to a rotation of the IMUs global frame on the horizontal plane caused, e.g., by magnetic disturbances. Correction to all other angles is negligible, as expected given the precise placement of the IMUs on the board. The angle α computed with NP and LP under the effect of the disturbance is quite noisy (top panel in Fig. 3), while its value remains close to the correct value of (90° for the pair of sensors represented in the figure) when computed with EP. The median and the upper and lower quartiles of the error between the measured angle and the ground truth are reported in Fig. 4 for each of the 5 pairs of IMUs. For all the considered pairs of IMUs, postprocessing with EP resulted in a significantly smaller median error and smaller error scattering. Summary statistics of the experiment (Table 2), computed by aggregating the error on the measurement of the 5 angles in a single time series, confirm that the error is significantly reduced both in RMS, mean, and median.

Table 2
Summary statistics of *Test 1*. For mean values, the standard deviation is reported between parentheses. For median values, lower and upper quartiles are reported between brackets. Statistics refer to the error computed over the union of the 5 different angles.

	NP	LP	EP
RMS [deg]	8.6	7.4	2.2
Mean [deg]	1.6 (8.5)	0.9 (7.4)	0.5 (2.1)
Median [deg]	1.2 [-0.2,4.9]	1.0 [-0.2,3.8]	0.4 [0.1,1.0]

The experiment in *Test 2* was repeated 3 times. In this case, the alignment of the IMUs with the anatomical axes was inevitably imperfect. As a consequence, multiple elements of ξ both for EP and EPSS settle on nonzero values (Fig. 5). The trials lasted about 120 seconds and the first 16 seconds were excluded from the time series to allow the state of EP and EPSS to settle. In this case, the error is defined as the difference between the measured angle and the subject carrying angle (16.4 degrees). LP and EP, which assume a carrying angle equal to 0, perform poorly and degrade the measure with respect to NP (Fig. 6). By looking at the aggregate statistics from the four trials, in Table 3, we see that EPSS, on the other hand, utilizing a more correct model improves both mean and median error. However, soft tissue artifacts and the more complex kinematics of the human arm, with respect to the simplified geometry assumed in *Test 1*, do not allow EPSS to achieve the same performance as EP in *Test 1*. Moreover, a larger variance affects the RMS error, which is slightly worse than with NP.

Finally, the experiment in *Test 3* was repeated 8 times. Each trial lasted about 60 seconds. The subject remained steady for about 16 seconds before beginning the flexion/extension drill, which lasted about 30 seconds. Imperfect alignment of the IMUs and soft-tissue

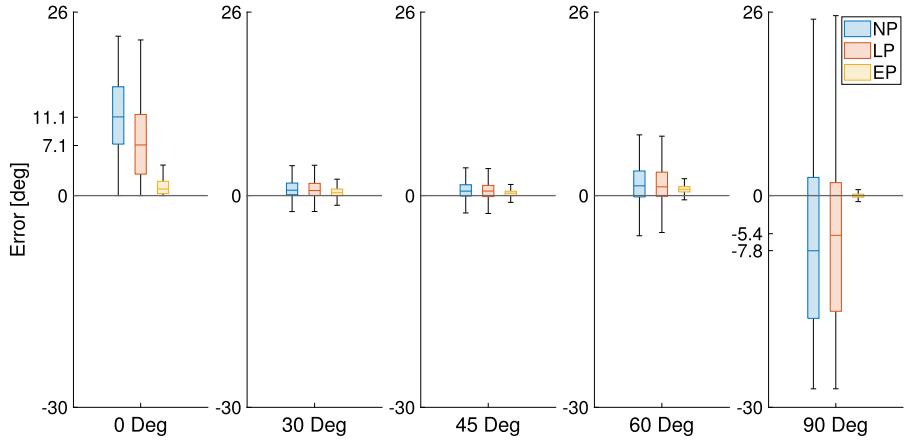

Fig. 4. Results of *Test 1*: error on the angle measured between $Sensor_1$ and $Sensor_2$. The central mark is the median, the boxes enclose the lower and upper quartiles.

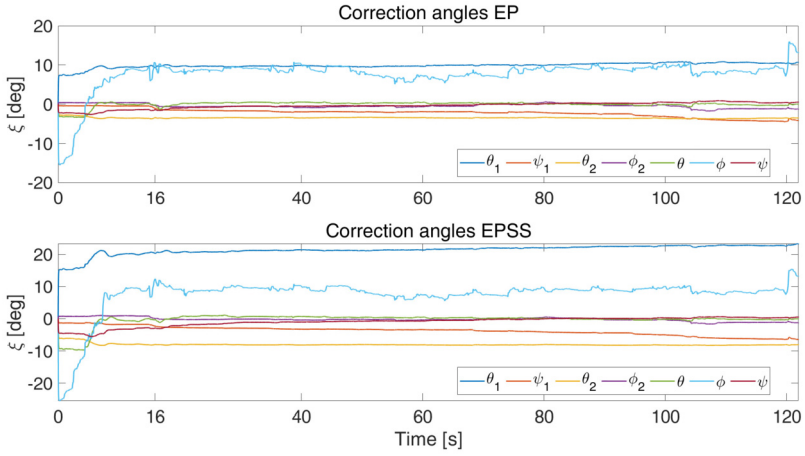

Fig. 5. Trajectory of ξ during Test 2.

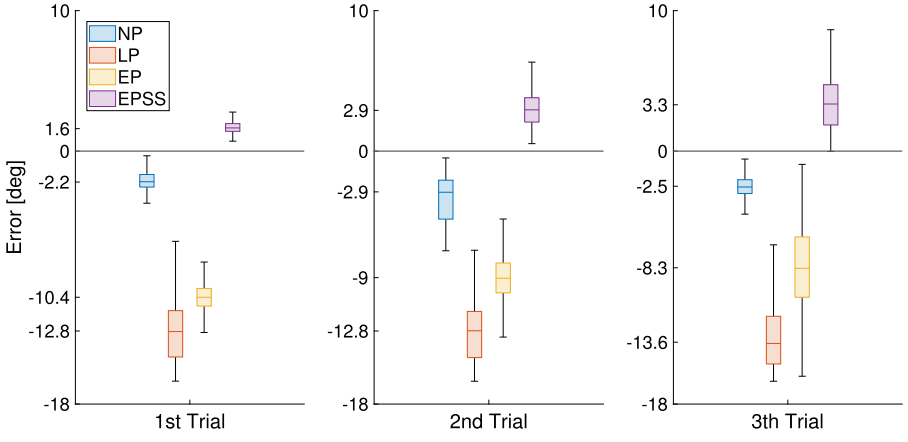

Fig. 6. Results of *Test 2*: error between the angle returned by the 4 computation methods, and the subject's flexion/extension angle, fixed at 16.4 degrees. Boxes represented as in Fig. 4.

Table 3
Summary statistics of *Test 2*. For mean values, the standard deviation is reported between parentheses. For median values, lower and upper quartiles are reported between brackets. Statistics refer to the error computed over the union of the 3 trials.

	NP	LP	EP	EPSS
RMS [deg]	2.8	12.8	9.6	2.9
Mean [deg]	-2.5 (1.2)	-12.5 (8.8)	-9.4 (6.4)	2.5 (5.1)
Median [deg]	-2.7 [-3.6,-2.1]	-12.6 [-14.7,-10.7]	-9.8 [-10.9,-8.9]	1.8 [1.4,2.3]

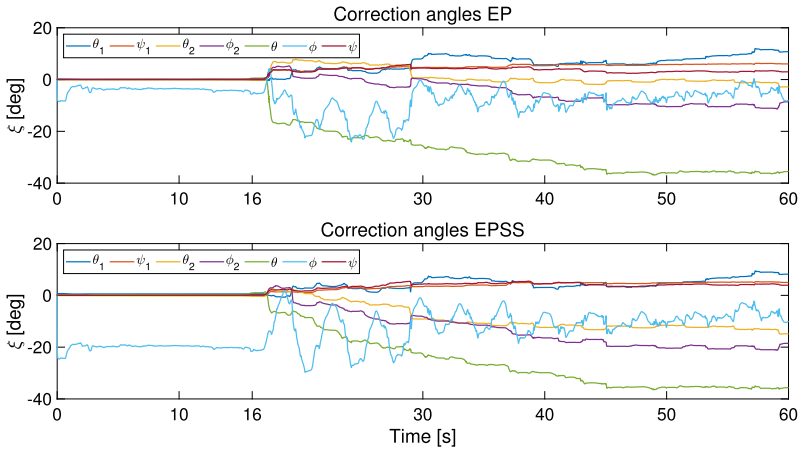

Fig. 7. Trajectory of ξ during Test 3.

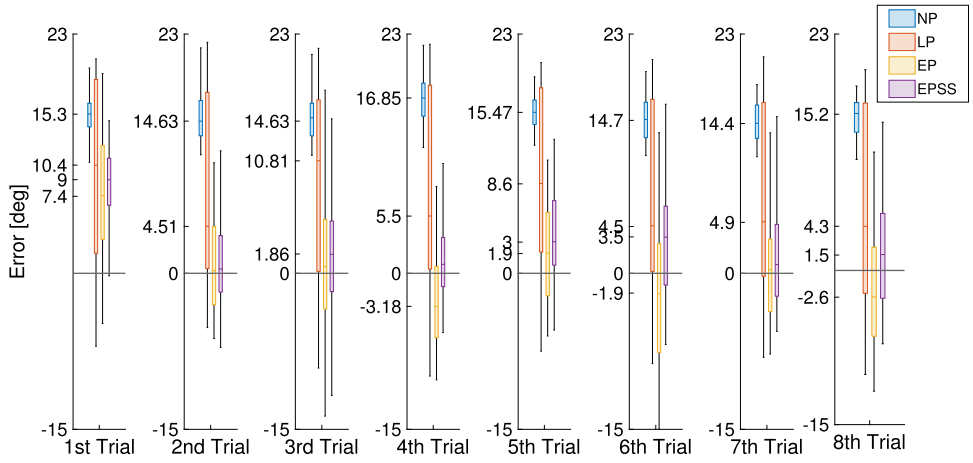

Fig. 8. Results of *Test 3*: error between the angle returned by the 4 computation methods, and the subject's flexion angle as measured with the optical tracking system. Boxes represented as in Fig. 4.

Table 4
Summary statistics of *Test 3*. For mean values, the standard deviation is reported between parentheses. For median values, lower and upper quartiles are reported between brackets. Statistics refer to the error computed over the union of the 8 trials.

	NP	LP	EP	EPSS
RMS [deg]	15.4	11.9	6.5	6.0
Mean [deg]	15.2 (2.1)	7.9 (8.8)	1.0 (6.43)	3.1 (5.1)
Median [deg]	15.3 [13.7,16.6]	6.3 [0.4,17.2]	0.7 [-3.5,4.8]	2.9 [-0.7,6.6]

artifacts induced by the motion of the arm this time excite most of the elements of state ξ (Fig. 7), which starts to settle onto its asymptotic value only after the subject starts moving (about 16 seconds from the beginning of the experiment in Fig. 7). When analyzing the error performance of the different algorithms therefore we excluded the first 16 seconds of data. Results are consistent among the 8 trials (Fig. 8), and in all cases, EPSS improves the error performance with respect to NP and LP. We note that in this test EP performed better than in *Test 2*, and achieved comparable results to EPSS. A more accurate assessment is reported in Table 4, which considers the statistics of the aggregate time series from the 8 trials. While both EP and EPSS perform much better than NP and LP, the mean and median values of EP are slightly better than those of EPSS, while the RMS errors are comparable.

4. Discussion

The tests were designed to evaluate different conditions under which the postprocessing algorithm could operate. *Test 1* allowed us to evaluate the performance of the algorithms in the absence of soft tissue artifacts, in a scenario where the carrying angle constraint of 0 is satisfied by construction, and evaluate the error against a reference that was characterized with extreme precision. This is, in other words, an accurate assessment of the best-case performance of the three algorithms EP, LP, and NP, when the kinematics of the process coincides with those assumed by the postprocessing. Fig. 4 clearly shows an improvement of EP over LP and NP. When the kinematic model is correct EP can achieve sub-degree mean and median error. Note that, with EP, we achieve an RMS error of 2.2 degrees despite the significant noise affecting the original signal, testified by the large error obtained with NP.

This is in line with the best results reported by competing algorithms in the literature [16], with the advantage, here, of having a purely postprocessing algorithm.

In contrast, *Test 2* was designed to evaluate the algorithm performance in the presence of soft-tissue artifacts and with the complexity of the human-arm geometry (but limiting the effects of elbow kinematics) while operating under similar electromagnetic and geometric conditions as in *Test 1*. Both LP and EP, being based on an erroneous model where the carrying angle is null, introduce an unnecessary bias in the measured angle, thus deteriorating the error performance with respect to the unprocessed signal returned by NP. On the other hand, EPSS, which utilizes a correct model of the carrying angle, provides a significant improvement, achieving a mean error of 2.3 degrees, improving significantly over LP. Note that, while the subject was instructed to keep the arm fully extended throughout the test, small variations of the elbow angle during the experiment were still likely due to the mechanical coupling between the degrees of freedom of the elbow. This probably explains the reduced performance of EPSS in *Test 2* with respect to EP in *Test 1*.

Finally, in *Test 3* we tested the proposed method with the subject executing a standard flexion/extension exercise, assessing the error against what to date is considered the gold standard for human motion analysis. Results are affected both by soft-tissue artifacts and, to some extent, by the imperfect positioning of the retroreflective markers with respect to the instantaneous centers of rotation of the shoulder and arm. Table 4 shows again that EP can improve the angle estimation compared with NP and LP, reducing mean and median error by almost an order of magnitude. In this case, adding the subject-specific carrying angle provides only a marginal improvement in the RMS error, and slightly deteriorates error mean and median values. The fact that EP, with a less precise kinematic model, performs comparably to EPSS might seem surprising. One should however consider that in the experimental conditions of *Test 2*, EP had no means to distinguish the presence of a nonzero carrying angle from an error in the alignment of the IMUs to the body segments longitudinal axes. This explains the large error of EP in this test. During *Test 3* instead, the subject was moving her arm both around the flexion/extension and, inevitably to some extent, the pronation/supination axes. The corresponding trajectories of the two IMUs in this case are geometrically distinct from those that would have been obtained with a null carrying angle. This is why the performances of EP and EPSS are in this case more similar. We can therefore conclude that EPSS is more robust than EP in assessing the elbow angle even in atypical motion such as in *Test 2*, but not necessarily better in more typical motion such as in *Test 3*. In our comparison with recent literature, it is worth noting that other studies have obtained comparable results. For example, the study presented by [5] obtained results similar to ours, but required a detailed calibration procedure prior to data acquisition, making it impractical for postprocessing. This is also true for [22] in which the calibration does indeed occur autonomously, but the subject must assume a "zero position" for this to happen. Our postprocessing method can instead improve measurement accuracy without the need for initial calibration, without requiring the subject to perform a zero position, nor knowledge of subject-specific parameters. Therefore, it can be applied to a dataset posterior to its acquisition, even if the protocol was not designed for postprocessing, or it can be inserted in a data-processing pipeline without any modification to the acquisition protocol. Note that, in *Test 2* and *Test 3*, subjects were not instructed to move at a specific speed. Very fast motion might, however, affect the performance of our and competing algorithms. This remains a direction for future research.

5. Conclusion

The postprocessing algorithm presented in this work does not require knowledge of the anthropometric parameters or calibration. Therefore, it can be used to clean previously acquired data without any modification to the acquisition protocol. Our tests show that the algorithm can reduce mean and median error in the computation of the elbow flexion/extension angle by almost an order of magnitude under typical conditions (*Test 3*), even without information on the carrying angle. This information is however important to reduce the error under atypical conditions (*Test 2*) e.g. when the subject is holding the arm fully extended.

Human and animal rights

The authors declare that the work described has been carried out in accordance with the Declaration of Helsinki of the World Medical Association revised in 2013 for experiments involving humans as well as in accordance with the EU Directive 2010/63/EU for animal experiments.

Funding

This work was partially supported by grant MISE-POC/EnTerQTraining (CUP C46I20000070006).

Author contributions

All authors attest that they meet the current International Committee of Medical Journal Editors (ICMJE) criteria for Authorship.

Declaration of competing interest

The authors declare that they have no known competing financial or personal relationships that could be viewed as influencing the work reported in this paper.

Acknowledgement

This work was partially supported by grant MISE-POC/EnTerQTraining (CUP C46I20000070006).

Appendix A. Supplementary material

Supplementary material related to this article can be found online at https://doi.org/10.1016/j.irbm.2024.100820.

References

[1] Fitoussi F, Diop A, Maurel N, Laasel EM, Ilharreborde B, Penneçot GF. Upper limb motion analysis in children with hemiplegic cerebral palsy: proximal kinematic changes after distal botulinum toxin or surgical treatments. J Child Orthop 2011;5:363–70. https://doi.org/10.1007/S11832-011-0365-Z.

[2] Parker VM, Wade DT, Hewer RL. Loss of arm function after stroke: measurement, frequency, and recovery. Int Rehabil Med 1986;8(2):69–73. https://doi.org/10.3109/03790798609166178. pMID: 3804600.

[3] Zhou H, Hu H. Human motion tracking for rehabilitation—a survey. Biomed Signal Process Control 2008;3(1):1–18. https://doi.org/10.1016/j.bspc.2007.09.001. https://www.sciencedirect.com/science/article/pii/S1746809407000778.

[4] Sorriento A, Porfido MB, Mazzoleni S, Calvosa G, Tenucci M, Ciuti G, et al. Optical and electromagnetic tracking systems for biomedical applications: a critical review on potentialities and limitations. IEEE Rev Biomed Eng 2020;13:212–32. https://doi.org/10.1109/RBME.2019.2939091.

[5] Cutti AG, Giovanardi A, Rocchi L, Davalli A, Sacchetti R. Ambulatory measurement of shoulder and elbow kinematics through inertial and magnetic sensors. Med Biol Eng Comput 2008;46(2):169–78. https://doi.org/10.1007/s11517-007-0296-5.

[6] Storm FA, Nair K, Clarke AJ, Van der Meulen JM, Mazzà C. Free-living and laboratory gait characteristics in patients with multiple sclerosis. PLoS ONE 2018;13(5):e0196463.

[7] Luinge HJ, Veltink PH. Measuring orientation of human body segments using miniature gyroscopes and accelerometers. Med Biol Eng Comput 2005;43(2):273–82.
[8] Euston M, Coote P, Mahony R, Kim J, Hamel T. A complementary filter for attitude estimation of a fixed-wing UAV. In: IEEE/RSJ international conference on intelligent robots and systems; 2008. p. 340–5.
[9] Madgwick SOH, Harrison AJL, Vaidyanathan R. Estimation of imu and marg orientation using a gradient descent algorithm. In: IEEE international conference on rehabilitation robotics; 2011. p. 1–7.
[10] Mahony R, Member S, Hamel T, Pflimlin J-M. Nonlinear complementary filters on the special orthogonal group. IEEE Trans Autom Control 2008;53:1203. https://doi.org/10.1109/TAC.2008.923738. http://ieeexplore.ieee.org.
[11] Sabatini AM. Kalman-filter-based orientation determination using inertial/magnetic sensors: observability analysis and performance evaluation. Sensors 2011;11:9182–206. https://doi.org/10.3390/s111009182. www.mdpi.com/journal/sensors.
[12] Tseng SP, Li W-L, Sheng C-Y, Hsu J-W, Chen C-S. Motion and attitude estimation using inertial measurements with complementary filter. In: 8th Asian control conference (ASCC); 2011. p. 863–8.
[13] Ligorio G, Sabatini AM. A novel Kalman filter for human motion tracking with an inertial-based dynamic inclinometer. IEEE Trans Biomed Eng 2015;62(8):2033–43. https://doi.org/10.1109/TBME.2015.2411431.
[14] Valenti RG, Dryanovski I, Xiao J. A linear Kalman filter for marg orientation estimation using the algebraic quaternion algorithm. IEEE Trans Instrum Meas 2016;65(2):467–81. https://doi.org/10.1109/TIM.2015.2498998.
[15] Majumder S, Deen MJ. A robust orientation filter for wearable sensing applications. IEEE Sens J 2020;20(23):14228–36. https://doi.org/10.1109/JSEN.2020.3009388.
[16] Caruso M, Sabatini AM, Laidig D, Seel T, Knaflitz M, Della Croce U, et al. Analysis of the accuracy of ten algorithms for orientation estimation using inertial and magnetic sensing under optimal conditions: one size does not fit all. Sensors 2021;21(7). https://doi.org/10.3390/s21072543. https://www.mdpi.com/1424-8220/21/7/2543.
[17] Nazarahari M, Rouhani H. 40 years of sensor fusion for orientation tracking via magnetic and inertial measurement units: methods, lessons learned, and future challenges. Inf Fusion 2021;68:67–84. https://doi.org/10.1016/j.inffus.2020.10.018. https://www.sciencedirect.com/science/article/pii/S1566253520303997.
[18] El-Gohary M, McNames J. Shoulder and elbow joint angle tracking with inertial sensors. IEEE Trans Biomed Eng 2012;59:2635–41. https://doi.org/10.1109/TBME.2012.2208750.
[19] Peppoloni L, Filippeschi A, Ruffaldi E, Avizzano CA. A novel 7 degrees of freedom model for upper limb kinematic reconstruction based on wearable sensors. In: 2013 IEEE 11th international symposium on intelligent systems and informatics (SISY); 2013. p. 105–10.
[20] Szczesna A, Pruszowski P. Model-based extended quaternion Kalman filter to inertial orientation tracking of arbitrary kinematic chains. SpringerPlus 2016;5(1):1–13.
[21] Seel T, Raisch J, Schauer T. Imu-based joint angle measurement for gait analysis. Sensors 2014;14(4):6891–909. https://doi.org/10.3390/s140406891. https://www.mdpi.com/1424-8220/14/4/6891.
[22] Muller P, Begin MA, Schauer T, Seel T. Alignment-free, self-calibrating elbow angles measurement using inertial sensors. IEEE J Biomed Health Inform 2017;21:312–9. https://doi.org/10.1109/JBHI.2016.2639537.
[23] Vitali RV, Cain SM, McGinnis RS, Zaferiou AM, Ojeda LV, Davidson SP, et al. Method for estimating three-dimensional knee rotations using two inertial measurement units: validation with a coordinate measurement machine. Sensors 2017;17(9). https://doi.org/10.3390/s17091970. https://www.mdpi.com/1424-8220/17/9/1970.
[24] Levangie PK, Norkin CC. Joint structure and function: a comprehensive analysis, 5e. New York, NY: McGraw-Hill Education; 2011.
[25] Luinge HJ, Veltink PH, Baten CT. Ambulatory measurement of arm orientation. J Biomech 2007;40:78–85. https://doi.org/10.1016/J.JBIOMECH.2005.11.011.
[26] Anglin C, Wyss U. Review of arm motion analyses. Proc Inst Mech Eng, H J Eng Med 2000;214(5):541–55.
[27] Roy PV, Baeyens JP, Fauvart D, Lanssiers R, Clarijs JP. Arthro-kinematics of the elbow: study of the carrying angle. Ergonomics 2005;48(11–14):1645–56.
[28] Windolf M, Götzen N, Morlock M. Systematic accuracy and precision analysis of video motion capturing systems—exemplified on the vicon-460 system. J Biomech 2008;41(12):2776–80. https://doi.org/10.1016/j.jbiomech.2008.06.024. https://www.sciencedirect.com/science/article/pii/S0021929008003229.
[29] Lobo-Prat J, Font-Llagunes JM, Gómez-Pérez C, Medina-Casanovas J, Angulo-Barroso RM. New biomechanical model for clinical evaluation of the upper extremity motion in subjects with neurological disorders: an application case. Comput Methods Biomech Biomed Eng 2014;17(10):1144–56.